Axonopathy in the Central Nervous System Is the Hallmark of Mice with a Novel Intragenic Null Mutation of *Dystonin*

Frauke Seehusen,* Kirsten Kiel,† Stefano Jottini,*,‡ Peter Wohlsein,* Andre Habierski,* Katharina Seibel,§ Tanja Vogel, Henning Urlaub, ††,‡‡ Martin Kollmar,§§ Wolfgang Baumgärtner,*,*** and Ulrike Teichmann†,1**

*Department of Pathology, University of Veterinary Medicine, D-30559 Hannover, Germany, †Animal Facility, §Department of Cellular Logistics, ††Bioanalytical Mass Spectrometry, and §§Department of NMR-Based Structural Biology, Research Group Systems Biology of Motor Proteins, Max Planck Institute for Biophysical Chemistry, D-37077 Göttingen, Germany, ‡Department of Animal Health, Pathology Unit, Faculty of Veterinary Medicine, University of Parma, I-43100, Italy, **Institute of Anatomy and Cell Biology, University of Freiburg, D-79104, Germany, ‡‡Bioanalytics, Department of Clinical Chemistry, University Medical Center Göttingen, D-37075, Germany, and ***Center for Systems Neuroscience, University of Veterinary Medicine, D-30559 Hannover, Germany

ABSTRACT Dystonia musculorum is a neurodegenerative disorder caused by a mutation in the *dystonin* gene. It has been described in mice and humans where it is called hereditary sensory autonomic neuropathy. Mutated mice show severe movement disorders and die at the age of 3–4 weeks. This study describes the discovery and molecular, clinical, as well as pathological characterization of a new spontaneously occurring mutation in the *dystonin* gene in C57BL/6N mice. The mutation represents a 40-kb intragenic deletion allele of the *dystonin* gene on chromosome 1 with exactly defined deletion borders. It was demonstrated by Western blot, mass spectrometry, and immunohistology that mice with a homozygous mutation were entirely devoid of the dystonin protein. Pathomorphological lesions were restricted to the brain stem and spinal cord and consisted of swollen, argyrophilic axons and dilated myelin sheaths in the white matter and, less frequently, total chromatolysis of neurons in the gray matter. Axonal damage was detected by amyloid precursor protein and nonphosphorylated neurofilament immunohistology. Axonopathy in the central nervous system (CNS) represents the hallmark of this disease. Mice with the *dystonin* mutation also showed suppurative inflammation in the respiratory tract, presumably due to brain stem lesion-associated food aspiration, whereas skeletal muscles showed no pathomorphological changes. This study describes a novel mutation in the *dystonin* gene in mice leading to axonopathy in the CNS. In further studies, this model may provide new insights into the pathogenesis of neurodegenerative diseases and may elucidate the complex interactions of dystonin with various other cellular proteins especially in the CNS.

KEYWORDS axonopathy; dystonia musculorum; dystonin deficiency; genomic deletion; spontaneous mutation

A spontaneously occurring mutant was described in the mouse, in which the gene *dystonin* was affected (Ledoux 2011). *Dystonin* (*Dst*) [human gene name, *DST*; former name, *bullous pemphigoid antigen 1* (*BPAG1*)] is a large cytoskeletal linker protein and crucial for maintaining cellular structural integrity (Young and Kothary 2008). Recent research in this field concentrates on the role of *dystonin* in central nervous tissue and neurological diseases, but not, however, on its parallel expression in musculature and skin.

Mice with a mutated *dystonin* gene develop a severe sensory neuropathy called dystonia musculorum (Duchen 1976). Characteristics are a progressive loss of coordination of the limbs (ataxia) and an early death (Kothary *et al.* 1988; Guo *et al.* 1995). There are only few reports about patients with mutations of the human *dystonin* gene (Giorda *et al.* 2004; Groves *et al.* 2010; Edvardson *et al.* 2012).

Several dystonin isoforms are generated from one genomic locus of 400 kb. They are expressed in the central nervous system (CNS) (predominant neuronal isoform "a," 617 kDa

doi: 10.1534/genetics.116.186932
Manuscript received January 18, 2016; accepted for publication July 3, 2016; published Early Online July 6, 2016.
Supplemental material is available online at www.genetics.org/lookup/suppl/doi:10.1534/genetics.116.186932/-/DC1.
[1]Corresponding author: Max Planck Institute for Biophysical Chemistry, Am Fassberg 11, D-37077 Göttingen, Germany. E-mail: ulrike.teichmann@mpibpc.mpg.de

and "n," 344 kDa), muscles (predominant muscle isoform "b," 834 kDa), and skin (predominant skin isoform "e," 302 kDa) (Figure 1). A central plakin domain is present in all isoforms and anchors dystonin to the plakin protein family (reviewed in Röper *et al.* 2002). Other domains involved in the binding of actin, intermediate filaments and microtubules, as well as a spectrin rod and a coiled-coil domain, are differentially present within the isoforms (Dalpé *et al.* 1998).

In addition to a targeted mutation of *dystonin* (Guo *et al.* 1995) and a transgenic insertion (Kothary *et al.* 1988), several naturally arising and only partially characterized mutant alleles are known in mice (listed in Pool *et al.* 2005). In human patients, mutation of genes ranges from single base pair (bp) deletion and point mutation to translocation (Giorda *et al.* 2004; Groves *et al.* 2010; Edvardson *et al.* 2012).

In this study, a new mutation in the murine *dystonin* gene, Dst:g.274762_314056del (with respect to genomic DNA), for simplicity called "*dt-MP*," is described. For this, detailed morphological and molecular analyses of the CNS and peripheral organs were performed. In this paper, we provide a detailed description of the first intragenic deletion allele of *dystonin* with exactly defined deletion borders. Additionally, we demonstrate that homozygous *dt-MP* mice are entirely devoid of the dystonin protein. The extension of the pathomorphological lesions in brain stem and spinal cord of mice with dystonia musculorum is precisely defined and axonopathy in the CNS represents the histologic hallmark of this entity.

Materials and Methods

Animals

Twenty-five breeding pairs of C57BL/6N were purchased as specific pathogen-free animals from a commercial breeder. The company assured providing siblings to maintain the inbred situation. After the first observation of the clinical phenotype, positive-proven carrier animals were intercrossed to produce phenotypically affected animals. After establishment of the genotyping protocol, homozygous *dt/dt* mice were generated from clinically unaffected heterozygous *dt/+* mating pairs.

Animals were killed between 13 and 18 days of age using carbon dioxide, except for perfusion fixations under general anesthesia with avertin (tribromoethanol) for the pathohistological investigation. Perfusion fixations were authorized by Az 33.9.42502-04/095/07 by the Niedersächsisches Landesamt für Verbraucherschutz und Ernährungsmittelsicherheit. All procedures were done in accordance with the German animal welfare law. Mice were housed in individually ventilated cages (Blue Line; Tecniplast, Hohenpeißenberg, Germany) with ad libitum access to standard mouse breeding chow and water.

Linkage analysis

In order to identify the genomic region with the gene of interest, proven-positive carrier C57BL/6N mice were mated with FVB/N mice (Supplemental Material, Figure S1). These N1 animals were then again crossed to proven-positive C57BL/6N mice. Genomic DNA from 12 affected and 20 unaffected F_2 offspring was analyzed at The Jackson Laboratory (Bar Harbor, ME) with a panel of 100 informative single nucleotide polymorphism markers in the C57BL/6N and FVB/N strains. The first scan identified a region between 0 and 64.7 Mb on the long arm of chromosome 1. In a second scan, 38 additional single nucleotide polymorphism markers narrowed down the region to between 20.8 and 49.6 Mb. Upon in silico analysis of all annotated genes and expressed sequence tags in this region, the *dystonin* gene was selected for further analysis. Complementary DNA (cDNA) of brain stem tissue from affected animals was investigated by PCR (Leung *et al.* 2001; Pool *et al.* 2005) and confirmed the assumption that indeed the *dystonin* gene was affected.

Isolation of genomic DNA and genomic analysis

Four littermates with the wild-type *+/+ dystonin* allele, as well as two C57BL/6N mice were used as controls for the deletion characterization on genomic DNA in five *dt-MP* animals. Tissue samples were digested overnight at 56° with 50 μl proteinase K (10 mg/ml) in tail lysis buffer (100 mM Tris HCl pH 8.5, 5 mM EDTA, 0.2% SDS, 200 mM NaCl). DNA extraction involved isopropanol precipitation followed by ethanol washing. The dried pellet was resuspended in 100 μl H_2O. To identify the deletion area and for genotyping, 1 μl genomic DNA solution, 1 μl dinucleotide triphosphate mix (10 mM) (Promega, Mannheim, Germany), 1 μl (10 pmol/μl) of each primer, 0.4 μl (two units) GoTaq G2 DNA polymerase, and 5 μl buffer (Promega) were used in a total volume of 50 μl in a Biometra T3 thermocycler. Primer sequences and PCR conditions can be found in File S1. In order to determine the exact deletion borders, sequencing of genomic DNA was performed by using an ABI 3100 Avant sequencer (Sanger *et al.* 1977). Primers were designed gradually according to the results of the last sequence. A PCR mix contained 50 ng genomic DNA, 3.2 pmol primer, and 8 μl reaction mix (ABI Prism Big Dye Terminator v3.0 Ready Reaction Cycle Sequencing Kit) in a total volume of 20 μl. The cycle sequencing program with denaturation at 95° for 30 sec, annealing at 50° for 10 sec, and elongation at 60° for 4 min was run for 25–30 cycles in a Biometra Trio thermocyler. The reaction mix was precipitated with 3 M sodium acetate and 100% ethanol, followed by 70% ethanol washing. The data analysis was carried out with the Sequencher program.

RT-PCR

Tissues from five *dt-MP* animals and six *dystonin +/+* littermates were flash frozen in liquid nitrogen. Lysis was performed with TRIzol followed by total RNA preparation with the RNeasy and RNAeasy plus mini kits combined with the RNase-Free DNase Set from QIAGEN (Valencia, CA). cDNA was transcribed from equal amounts of RNA with the superscript kit from Stratagene (La Jolla, CA) and subjected to PCR

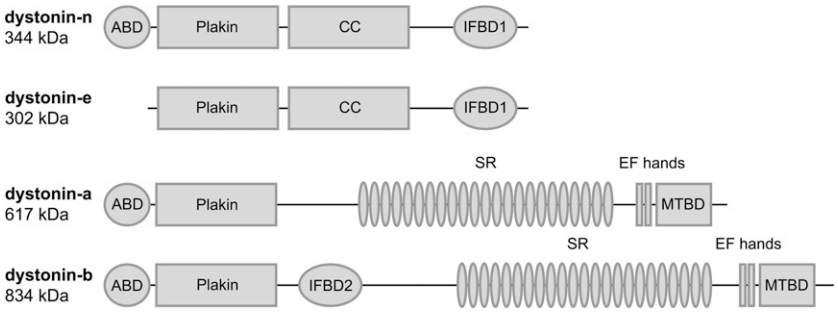

Figure 1 Structure of different murine dystonin isoforms. The structure of the different dystonin isoforms is shown (adapted from Goryunov *et al.* 2007). ABD, actin-binding domain; CC, coiled-coil domain; EF hands, EF hand-calcium binding domains; IFBD1/2, intermediate filament binding domain 1/2; MTBD, microtubule binding domain; SR, spectrin rod domain.

assays in a Biometra T3 thermocyler. Primer sequences and PCR conditions can be found in File S1.

Protein purification

Flash-frozen tissues from three *dystonin* +/+ mice, one C57BL/6N wild-type mouse, one heterozygous *dt*/+ animal, and four *dt-MP* mutants were lysed in native lysis buffer (50 mM Tris, pH 8, 100 mM NaCl, 5 mM $MgCl_2$, 5 mM DTT, complete protease inhibitor cocktail). The lysis was assisted by SilentCrushers (Heidolph Instruments, Schwabach, Germany) at 26,000 rpm for 20 sec at 4°. For storage at −80°, 250 mM sucrose was added to the supernatant after centrifugation of cellular debris. SDS buffer (80 mM Tris HCl, pH 6.8, 4% SDS, 0.5 M sucrose, 50 mM DTT, very little bromphenol blue) was added for a final protein concentration of 2–5 μg/μl. The protein lysates were processed for Western blot and mass spectrometry (MS). No differences were observed between *dystonin* +/+ and *dt*/+ animals.

Western blot

SDS/PAGE was performed with 10 μl per lane on gradient gels (NuPAGE Novex Tris-Bis Mini Gel, Invitrogen, Thermo Fisher Scientific, Darmstadt, Germany) running at 200 V for 80 min. After separation of probes, gels were equilibrated in electrophoresis buffer (0.2 mM glycine, 24.7 mM Tris base, 3.5 mM SDS) with 20% methanol. Proteins were transferred in electrophoresis buffer with 20% methanol on a nitrocellulose membrane overnight at 4° and 50 mA. Membranes were washed with tris-buffered saline (TBS) (0.15 M NaCl, 0.6 mM Tris base, 16 mM Tris HCl) and incubated in TBS with 5% skim milk powder as blocking solution. Incubation of the primary antibody 18024 occurred in blocking solution with 0.05% NaN_3 overnight at 4°. Membranes were washed three times in TB before being incubated with the secondary antibody (rabbit/mouse IRDye 800/680, dilution 1:40,000) in blocking solution for 45 min. After three washing steps in TBS, bands were detected on dried membranes with the LI-COR Odyssey Imaging System (LI-COR Biotechnology, Bad Homburg, Germany).

MS

Proteins were separated by one-dimensional SDS/PAGE (4–12% NuPAGE Bis-Tris gel, Invitrogen, Thermo Fisher Scientific), and the entire lane of the Coomassie blue-stained gel was cut into 23 slices. All slices were reduced with 10 mM DTT for 55 min at 56°, alkylated with 55 mM IAA for 20 min at 26° and digested with modified trypsin (Promega) overnight at 37°. Tryptic peptides were injected into a C18 precolumn (1.5 cm, 360 μm o.d., 150 μm i.d., Reprosil-Pur 120 Å, 5 μm, C18-AQ; Dr. Maisch, Ammerbuch-Entringen Germany) at a flow rate of 10 μl/min. Bound peptides were eluted and separated on a C18 capillary column (15 cm, 360 μm o.d., 75 μm i.d., Reprosil-Pur 120 Å, 5 μm, C18-AQ; Dr. Maisch) at a flow rate of 300 nl/min, with a gradient from 7.5 to 37.5% acetonitrile in 0.1% formic acid for 50 min using an Agilent 1100 Nano-Flow LC system (Agilent Technologies, Waldbronn, Germany) coupled to an LTQ-Orbitrap XL hybrid mass spectrometer (Thermo Electron, Thermo Fisher Scientific). The mass spectrometer was operated in the data-dependent mode to automatically switch between MS and MS/MS acquisition. Survey MS spectra were acquired in the Orbitrap (m/z 350–1600) with the resolution set to 30,000 at m/z 400 and automatic gain control target at 5 × 105. The five most intense ions were sequentially isolated for collision-induced dissociation MS/MS fragmentation and detection in the linear ion trap. Ions with single and unrecognized charge states were excluded. Raw data were analyzed with the Mascot search engine for peptide and protein identifications. Results were transferred to scaffold 3 for further analysis.

Histology, immunohistology, and electron microscopy

CNS tissues of 5 affected *dt-MP* mice, 5 *dystonin* +/+ littermates, and 2 C57BL/6N wild-type animals were investigated. Additionally, peripheral organs of 20 *dt-MP* animals, in most cases littermates of the same age, and 21 control animals (10 *dystonin* +/+ mice, 9 heterozygous *dt*/+ mice, and 2 C57BL/6N animals) were investigated histologically. No differences were observed between *dystonin* +/+ and *dt*/+ animals.

Tissue samples of the CNS, heart, skeletal muscle, skin, lung, nasal cavity, thymus, lymph nodes, spleen, liver, gastrointestinal tract, endocrine organs, urogenital tract, and peripheral nerves were fixed in 10% buffered formalin, embedded in paraffin wax, and cut at 2–3 μm. All tissue sections were stained with hematoxylin/eosin (H&E). Selected localizations were additionally stained with Luxol Fast Blue (LFB) and Bielschowsky's silver. Primary antibodies used are as follows: dystonin/BPAG1 (polyclonal, LS-C123425/70642; LifeSpan Biosciences, Seattle, WA;

1:400), β-amyloid precursor protein (monoclonal, MAB348 Merck Millipore, Darmstadt, Germany; 1:800, microwave pretreatment), phosphorylated neurofilaments (monoclonal, SM312; Covance, Emeryville, CA; 1:8000), nonphosphorylated neurofilaments (monoclonal, SM311; Covance; 1:8000, microwave pretreatment), and myelin basic protein (polyclonal, AB980; Merck Millipore; 1:800) according to a standard immunohistological protocol (Seehusen and Baumgärtner 2010).

For transmission electron microscopy (TEM), mice were anesthetized with avertin (tribromoethanol). Following injection of 5 IU heparin-sodium, the animals were perfused with 2.5% glutaraldehyde. Tissue samples of brain, spinal cord, peripheral nerves, and skeletal and cardiac musculature were embedded in Epon according to standard protocols (Bock *et al.* 2013).

Statistical analysis

Statistical analysis of the occurrence of pathological changes in peripheral organs between the *dt-MP* mice and controls was made by Fisher's exact test (www.graphpad.com), considering a *P*-value of ≤ 0.05 as a statistically significant change.

Data availability

The authors state that all data necessary for confirming the conclusions presented in the article are represented fully within the article.

Results

Clinical findings

In litters of two C57BL/6N breeding pairs from a commercial breeding company, ~25% of the offspring displayed neurological disorders. Neurological symptoms started at ~12 days of age and progressively increased in severity (Figure 2). Both sexes were equally affected. The first clinical sign was a wrist flexion of the forelimbs, resulting in coordination abnormalities. Within the following days, also the hindlimbs showed an overextension, eventually resulting in ataxic movements and a progressive disability to walk or get up after falling down. Furthermore, the whole body displayed a hyperextented position. The general body condition decreased severely, as seen from a hunched posture, weight loss, closed eyes, and reduced motor activity. Death occurred around the age of 19–24 days, before the animals reached adulthood and breeding maturity. The phenotype was passed to the next generation by mating healthy littermates. Assuming a monogenic recessive autosomal mutation, we performed a molecular and morphological investigation of animals between 13 and 22 days of age.

Identification of the genomic region

First, we identified a putative genomic region by linkage analysis (Figure S1). The phenotype had previously been restored in offspring from intercrosses of healthy carrier animals to wild-type FVB/N mating partners. The genomes of affected mice were compared to those of healthy littermates via a comprehensive SNP panel. It was predicted from the C57BL/6N-FVB/N hybrid genomes that a 28-Mb region on the long arm of mouse chromosome 1 might be affected. We analyzed expressed sequence tags and genes within this area *in silico* and identified the murine *dystonin* gene as a strong candidate.

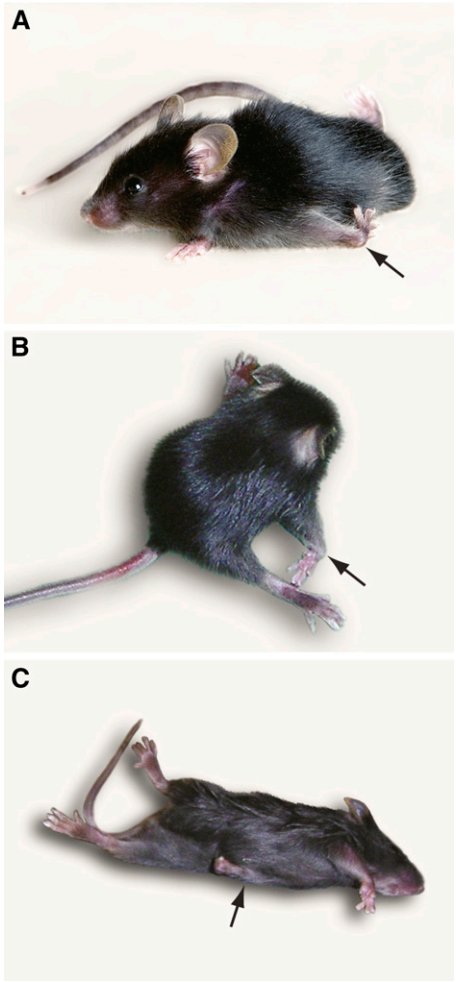

Figure 2 Clinical findings in *dt-MP* mice. Affected mice show a severe neuromuscular disorder beginning with a wrist flexion of the forelimbs (arrows) (A and B). The hindlimbs are splayed (B). The animals have severe difficulties in turning after being placed on their backs (C). Note that the left forelimb (arrow) is extended along the body axis instead of being used for turning over the left shoulder.

Genomic characterization of the mutant allele

With PCR primers binding in exon 43 of the wild-type *dystonin* genomic locus (Pool *et al.* 2005), a 613-bp product was amplified from the DNA of healthy mice only (Figure 3A). This exon is coding for the intermediate filament binding domain 2 (IFBD2).

It was concluded that the murine *dystonin* gene was indeed affected and that at least parts of it were deleted in phenotypically affected mice. To assess the entire dimension of the

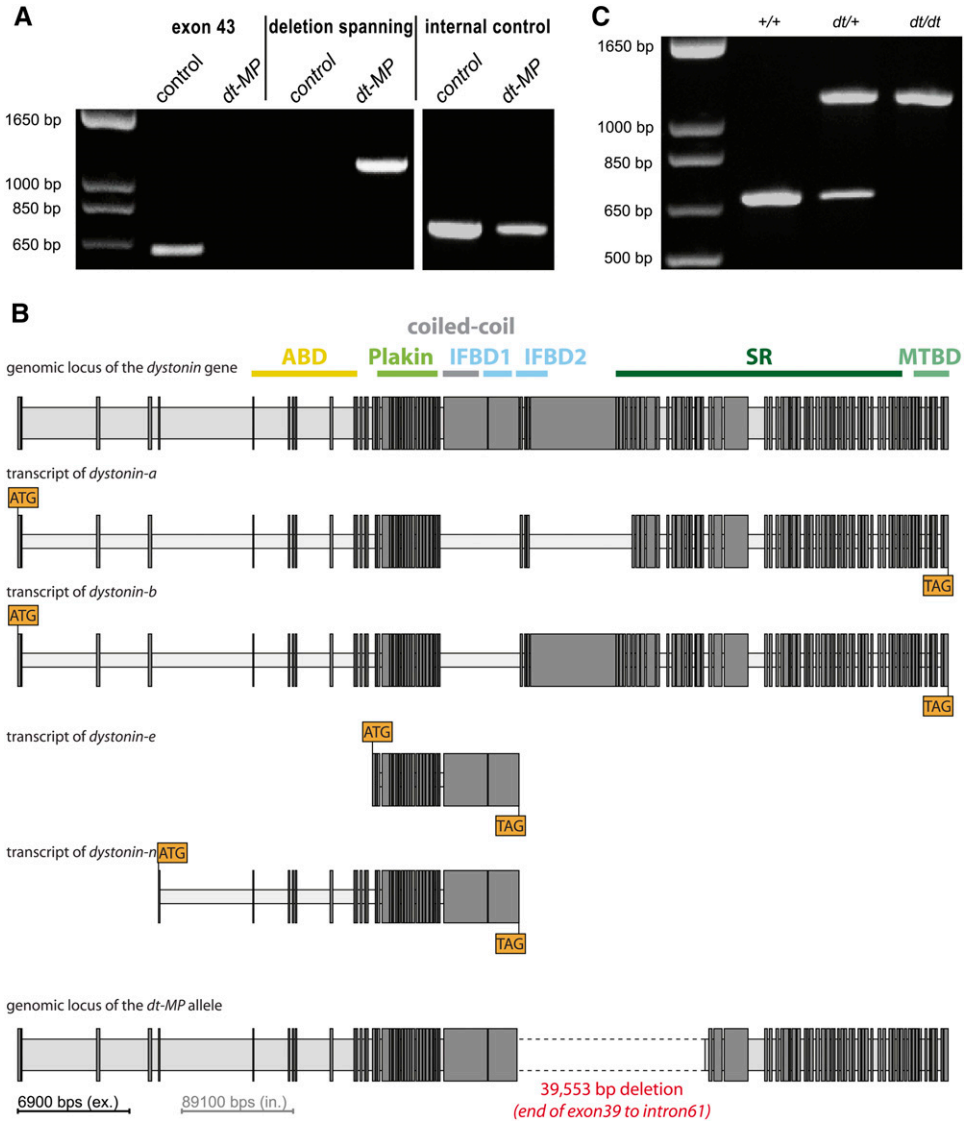

Figure 3 (A) Molecular identification of the deletion area. PCR on genomic DNA of control and *dt-MP* mice. Lanes 1 and 2 show exon 43 is amplified in control, but not in *dt-MP* mice. Lanes 3 and 4 show primers spanning over the deletion (from exon 39 to intron 61) do not amplify genomic DNA in control, but in *dt-MP* mice. Lanes 5 and 6 show dystonin nt 272159–272908 as internal control. (B) Structure of *dystonin* alleles. Structure of the genomic region of mouse *dystonin* as obtained with WebScipio (Hatje *et al.* 2013). Dark gray and light gray boxes represent exons and introns, respectively. Introns have been scaled down by a factor of 12.9 for clarity. ATG and TAG represent start and stop codons, respectively, of the indicated isoforms. Functional domains are illustrated in the wild-type allele on top for better orientation (ABD, actin-binding domain; IFBD, intermediate filament binding domain; MTBD, microtubule-binding domain; SR, spectrin repeats). The scheme on the bottom represents the genomic region of the *dt-MP* allele that misses 39,553 bp in the middle of the gene including the *dystonin-e/n*-specific stop codon. For nucleotide and amino acid sequences in the wild-type mouse *dystonin* and *dt-MP* alleles, see Figure S2. (C) Genotyping of the *dystonin* locus. A 700-bp band is amplified from the wild-type allele only. A 1200-bp band characterizes the mutant allele.

missing region, we performed further PCR analysis in up- and downstream directions. The deletion spanned ~40 kb corresponding to 10% of the 400-kb genomic *dystonin* locus (399,318 bp, GenBank accession no. NC_000067.5). This finding was confirmed by using primers up- and downstream of the deleted region from exon 39 to intron 61. A 1200-bp product was amplified from the DNA of affected animals only, not of healthy littermates. Sequencing determined the deletion borders at nucleotide 274,762 (with respect to gene) at the end of exon 39 and at nucleotide 314,056 (with respect to gene) in intron 61. In total, 39,553 bp are missing entirely, resulting in a 359,762-bp allele in the genome of *dt-MP* mutant animals (Figure 3B). Details about the sequences flanking the deletion are given in Figure S2.

This is the first mutant allele of the murine *dystonin* gene that was characterized exactly on the molecular, nucleotide-based level. The intragenic deletion was precisely defined and we named the new allele *dt-MP*.

After determination of the deletion with primers up- and downstream of the deleted area, a genotyping protocol was set up (Figure 3C). All affected animals had the 1200-bp band spanning over the genomic deletion, indicating the *dt/dt* genotype. Presence of the wild-type *dystonin* allele in healthy littermates was proven by amplification of a 700-bp element within the deleted region. DNA from healthy animals had either both the 1200-bp and the 700-bp bands (indicating the *dt/+* genotype) or the 700-bp band only (indicating the +/+ genotype).

Heterozygous *dt/+* mice were intercrossed and gave rise to offspring with the dystonia musculorum phenotype. The ratios of genotypes (~25% of the offspring, independent of gender) in the litters were according to the expected Mendelian ratio. In addition, we used the genotyping protocol to investigate the DNA of the originally purchased 25 C57BL/6N breeding pairs. Unambiguously, only the two breeding pairs that gave rise to phenotypically apparent offspring had the *dt/+* genotype. All

other breeding pairs were +/+ at the *dystonin* locus (Figure S3).

RT-PCR analyses of the different dystonin isoforms

The different isoforms *dystonin-a*, *-b* and *-e/n* were analyzed in cDNA of brain stem, heart, and skin. As reported for +/+ animals (Leung *et al.* 2001), *dystonin-a*, *-b*, and *-e* were present in brain stem, heart, and skin in differing intensities (Figure 4A). In *dt/dt* mice, no transcript of either *dystonin* isoform could be detected (Figure 4B).

Protein expression

The polyclonal antibody AB18024 was used for the Western blots to detect dystonin protein in brain stem tissue [generous gift from Ronald Liem (Goryunov *et al.* 2007)] of a *dt-MP* animal (genotype *dt/dt*) and a healthy *dt/+* animal as control. The antibody is directed against the plakin domain of the dystonin protein that is present in all isoforms.

In control tissue, we detected two high molecular weight bands of >200 kDa in the brain stem. No dystonin protein of wild-type size was detected in brain stem tissue of the *dt-MP* animal (Figure 5).

The genomic situation in *dt-MP* mice with a new putative premature stop codon TAA in the former intronic region of intron 61 would allow for the possibility that lower weight, truncated protein fragments are generated from the mutated allele. However, we were unable to detect lower weight protein fragments with this antibody in the brain stem of *dt-MP* animals. To further confirm this finding, the protein expression was analyzed by MS. In control brain stem tissue, 39 peptides matching dystonin were detected. Matching peptides were present both in high molecular as well as in lower molecular weight bands, the latter most probably representing fragmentation products. In contrast, dystonin-specific peptides could not be detected in brain stem tissue extracts of *dt-MP* mice. From these findings it was concluded that *dt-MP* mice do not produce full-length or truncated forms of the dystonin protein.

To further substantiate these findings, an immunohistological investigation of the CNS, skin, skeletal muscle, and peripheral nerve was performed with a commercially available polyclonal anti-dystonin antibody. In all investigated tissues, immunoreactivity could be detected in control (+/+) mice, whereas *dt-MP* mice showed a severe downregulation of the antigen expression (Figure 6).

Neuroaxonal degeneration in central nervous tissue of dt-MP animals

Macroscopic lesions in the CNS were not found at necropsy in any of the animals investigated. The CNS of the control animals was histologically without pathological findings. However, all *dt-MP* animals displayed neurodegenerative changes predominantly in the brain stem and spinal cord, and rarely in the cerebellum. Changes were located in the reticular formation and the spinal cord with decreasing frequency from the cervical to the lumbar spinal cord. In the white matter of the spinal cord, changes were most prominent in ventrolateral and ventral funiculi (including the corticospinal, reticulospinal, and spinothalamic tracts). They were also found less frequently in the dorsal and dorsolateral funiculi. In ventral rootlets swollen axons and dilated myelin sheaths were occasionally detected. Neuronal changes were seen mostly bilaterally and symmetrically, located in mesencephalic and metencephalic gray matter, including anterior pretectal nucleus, retroethmoid thalamic nucleus, spinal trigeminal nucleus, raphe nuclei, gigantocellular reticular nucleus, and dorsal root ganglia (all sensory neurons), pontine nuclei and ventral horns of the spinal cord (motor neurons). Accordingly, several mainly sensory nuclei were affected (Figure 7).

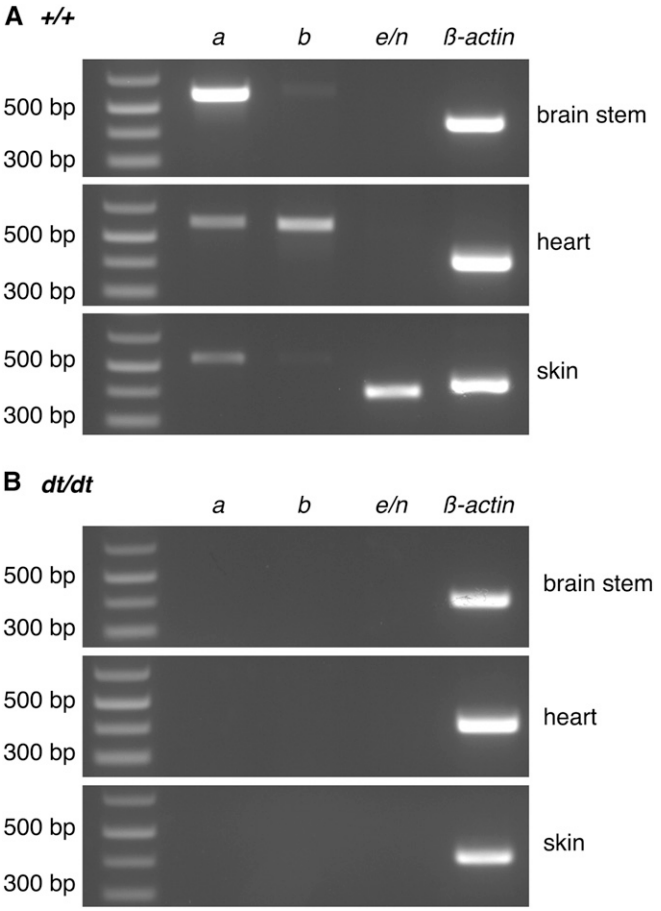

Figure 4 Detection of the *dystonin* isoforms in cDNA of different tissues. (A) In the brain stem of control (+/+) animals *dystonin-a* could be strongly detected, whereas *dystonin-b* was present very weakly. From control heart cDNA, both *dystonin-a* and *-b* were amplified with the *b* isoform giving the stronger band. In skin tissue, *dystonin-e/n* was clearly and *dystonin-a* weakly present. (B) In brain stem, heart, and skin of *dt-MP* (*dt/dt)* animals, neither *dystonin* isoform was detected. Controls in A and B: *β-actin*.

Axonal spheroids could be found in the white matter. In the H&E stain, they appeared as variably sized, round to irregular, strongly to weakly eosinophilic axonal swellings. Occasionally, myelinophages occurred in dilated myelin sheaths (Figure 8, A and B). Furthermore, they

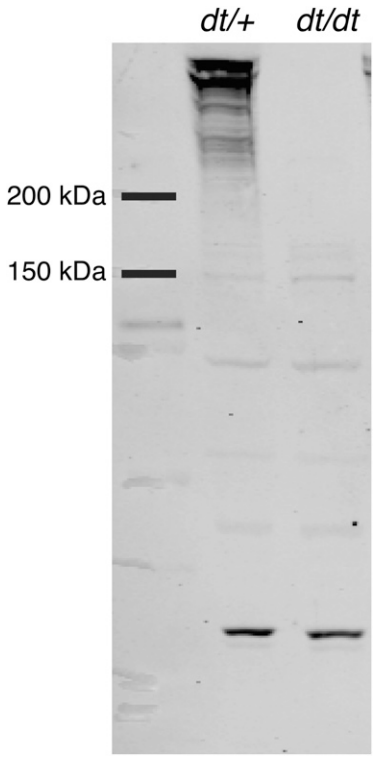

Figure 5 Western blot with the polyclonal antibody 18024 on brain stem tissue. Two high molecular weight bands of >200 kDa are detectable in tissue of a control (*dt*/+) animal, but missing in tissue of a *dt*/*dt* littermate. Since the antibody 18024 is directed against the plakin domain, other plakin family proteins than dystonin might be detected.

showed typical argyrophilia in Bielschowsky's silver stain (Figure 8, C and D).

Gray matter lesions were observed less frequently and consisted of total chromatolysis with cellular swelling, eccentrically located nucleus, and accumulated argyrophilic fibrillar cytoplasmic material in single neurons of the brain and spinal cord.

Neurodegenerative changes of *dt-MP* animals were further characterized by using immunohistology. The majority of spheroids stained positively for β-amyloid precursor protein (β-APP), phosphorylated neurofilament (p-NF), and nonphosphorylated neurofilament (n-NF) confirming that axonal damage is a primary central hallmark in *dt-MP* animals (Table 1 and Figure 8, E–H). Many chromatolytic neurons revealed marked accumulation of p-NF.

Using LFB stain and immunohistological detection of myelin basic protein, intact myelin formation was confirmed. Using TEM, the axonal spheroids were characterized by an enlarged diameter, accumulated neurofilaments, and numerous mitochondria as well as electron-dense bodies and tubulevesicular profiles. At the periphery a thin layer of myelin material was present. Additionally, in spinal cords of dt-MP mice, several axons in the white matter showed a hyper- or dysmyelination with a thickened myelin sheath and redundant myelin folding as well as separation of myelin layers (Figure 9).

Lesions in peripheral organs

Histological analysis of peripheral tissues of 21 *dystonin* wild-type and heterozygous animals and 20 *dt-MP* animals (in most cases littermates of the same age) including lymphoid tissues, endocrine organs, and tissues of the gastrointestinal, urogenital, and respiratory system was performed. Twelve of the 20 *dt-MP* (60%) animals exhibited mild to moderate suppurative inflammatory changes in the lungs (Figure S4). In contrast, only one (5%) of the 21 control animals showed a mild suppurative pneumonia. Statistical analysis confirmed that suppurative pneumonia occurred significantly more frequently in *dt-MP* animals compared to controls (*P*-value 0.0002). Additionally, in 9 *dt-MP* and 7 *dystonin* wild-type animals a mild suppurative lymphadenitis was detected. Three *dt-MP* animals and only one control animal possessed a mild-to-moderate suppurative rhinitis, whereas a mild tracheitis and conjunctivitis was only seen in one *dt-MP* animal.

Peripheral nerves and skeletal muscles were without significant histopathological changes in H&E stained tissue sections in *dt-MP* animals and controls, respectively.

To further characterize subtle changes in peripheral nerves, sciatic and brachial nerves of two *dt-MP* and two *dystonin* +/+ control mice (littermates) were collected and investigated via TEM. Mutant mice showed a wider variation in the axonal diameter of the peripheral nerves and single spheroids with an accumulation of cell organelles (Figure 10).

No lesions were identified in cardiac and skeletal muscles of affected animals by TEM.

Discussion

In the present study, a new mutant allele of the mouse *dystonin* gene, *dt-MP*, was characterized on a clinical, molecular, and pathologic level. The new mutant allele on chromosome 1 of the murine genome was characterized by a deletion of ~40 kb. Western blotting, MS, and immunohistology showed a lack of the dystonin protein expression in homozygous *dt-MP* mice. Affected mice exhibited severe neurological signs and weight loss and died before maturation. Histopathological and ultrastructural studies showed neurodegenerative changes predominately of the brain stem and spinal cord. The immunoreactivity of axons for transport proteins like β-APP and intermediate filaments indicated axonal damage as the pathogenetic hallmark of the disease.

In contrast to other mutant *dystonin* alleles (Goryunov *et al.* 2007), the deletion of a large genomic area represents a unique feature of the *dt-MP* allele. The loss of a 40-kb segment of the 400-kb wild-type genomic *dystonin* locus in the described new mutant allele represents one of the largest deletion alleles of *dystonin* after spontaneous mutation so far. The formerly reported *dt-Alb* allele is a deletion combined with an integration of a retroviral element and other spontaneous mutant alleles such as dt^{24J}, dt^{27J}, and dt^{Frk} are not further characterized (Pool *et al.* 2005; Goryunov *et al.* 2007).

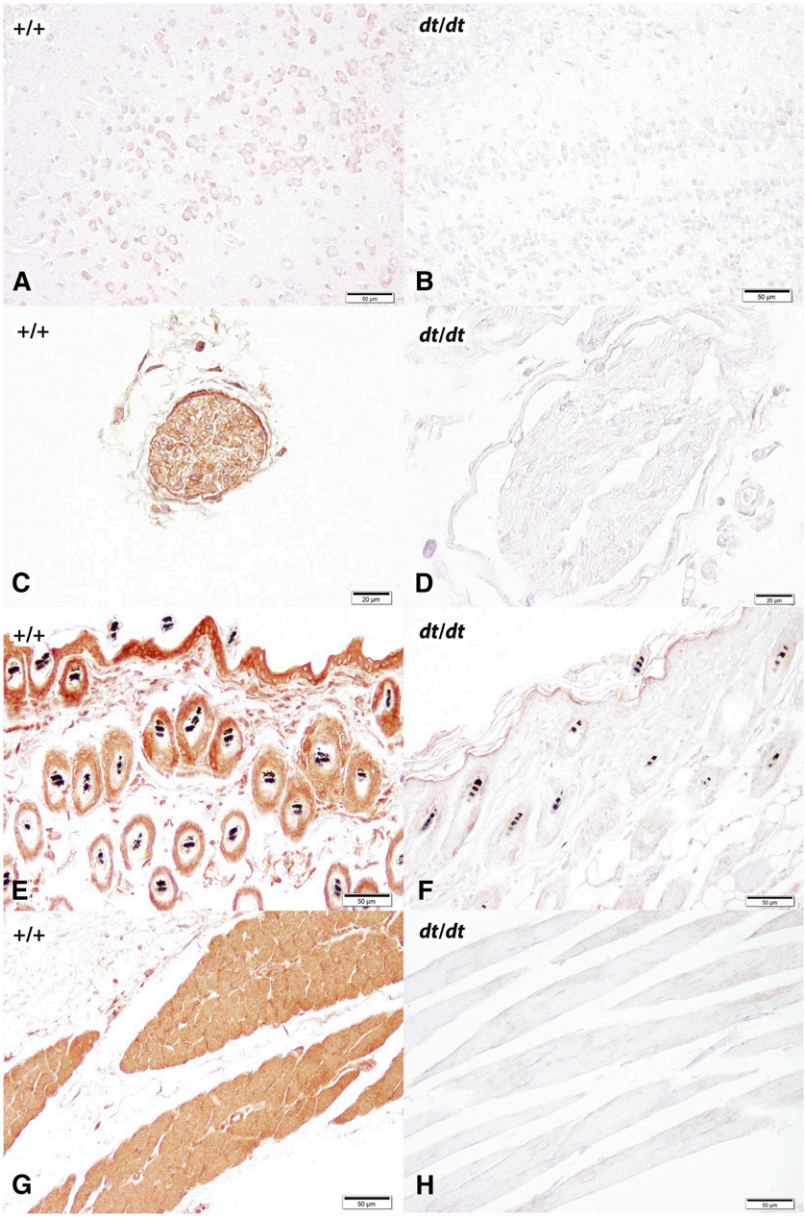

Figure 6 Dystonin immunohistology. Immunohistological investigation with the polyclonal anti-dystonin antibody LS-C123425/70642 on brain tissue, peripheral nerve, haired skin, and skeletal muscle of *dystonin* control mice (+/+) and *dt-MP* (*dt/dt*) animals. (A) Bulbus olfactorius of a control (+/+) animal with positively stained cytoplasm of neurons. Bar, 50 μm. (B) Bulbus olfactorius of a *dt-MP* mouse with only a weak cytoplasmic signal. Bar, 50 μm. (C) Sciatic nerve of a control (+/+) animal with positively stained nerve fibers. Bar, 20 μm. (D) Sciatic nerve of a *dt-MP* mouse without immunoreactivity. Bar, 20 μm. (E) Haired skin of a control (+/+) animal with positively stained keratinocytes and follicular epithelial cells. Bar, 50 μm. (F) Haired skin of a *dt-MP* mouse with only a weak cytoplasmic immunoreactivity of superficial keratinocytes. Bar, 50 μm. (G) Skeletal muscle of a control (+/+) animal with positively stained muscle fibers. Bar, 50 μm. (H) Skeletal muscle of a *dt-MP* mouse with only a multifocal weak cytoplasmic signal of myocytes. Bar, 50 μm.

The affected protein domains IFBD1 and IFBD2 are characteristic of the skin and muscle isoforms of dystonin, respectively, but not of the predominant neuronal isoform dystonin-*a* (Goryunov *et al.* 2007). Therefore, a skin or muscle phenotype consisting of epidermolysis bullosa-like changes or intrinsic muscle weakness seems more likely. According to this, skeletal musculature was affected on the ultrastructural level in another mouse mutant suffering from dystonia musculorum (Dalpé *et al.* 1999). In contrast to the brain, however, muscular tissue is characterized by huge amounts of actin and myosin filaments, and compared to the CNS, different molecules are in charge of proper filament organization. This redundancy may therefore compensate for the loss of dystonin in the heart and prevent a more severe cardiac or muscular phenotype. Candidates for redundancy are desmoplakin, plectin, and MACF1, which all share significant functional homologies to dystonin. In hearts of dt^{Tg4} mutant mice, desmoplakin was upregulated in contrast to wild-type control animals (Boyer *et al.* 2010).

By Western blot analysis, a plakin-domain-bearing protein was detected as high molecular weight bands in control animals. These two bands are missing in *dt-MP* mice. The two bands in the controls may result from the two isoforms dystonin-*a* (617 kDa) and dystonin-*b* (834 kDa), which are both present in brain tissue (Leung *et al.* 2001). The peptides detected by mass spectrometry in high molecular weight bands in control animals matched to the dystonin-*b* isoform. This finding confirms the assumption that the plakin-domain-bearing protein was indeed dystonin. According to the Western blot and MS data, a true null allele emerged in *dt-MP* mice. The immunohistological investigation using an anti-dystonin antibody revealed a positive reaction in brain, skin,

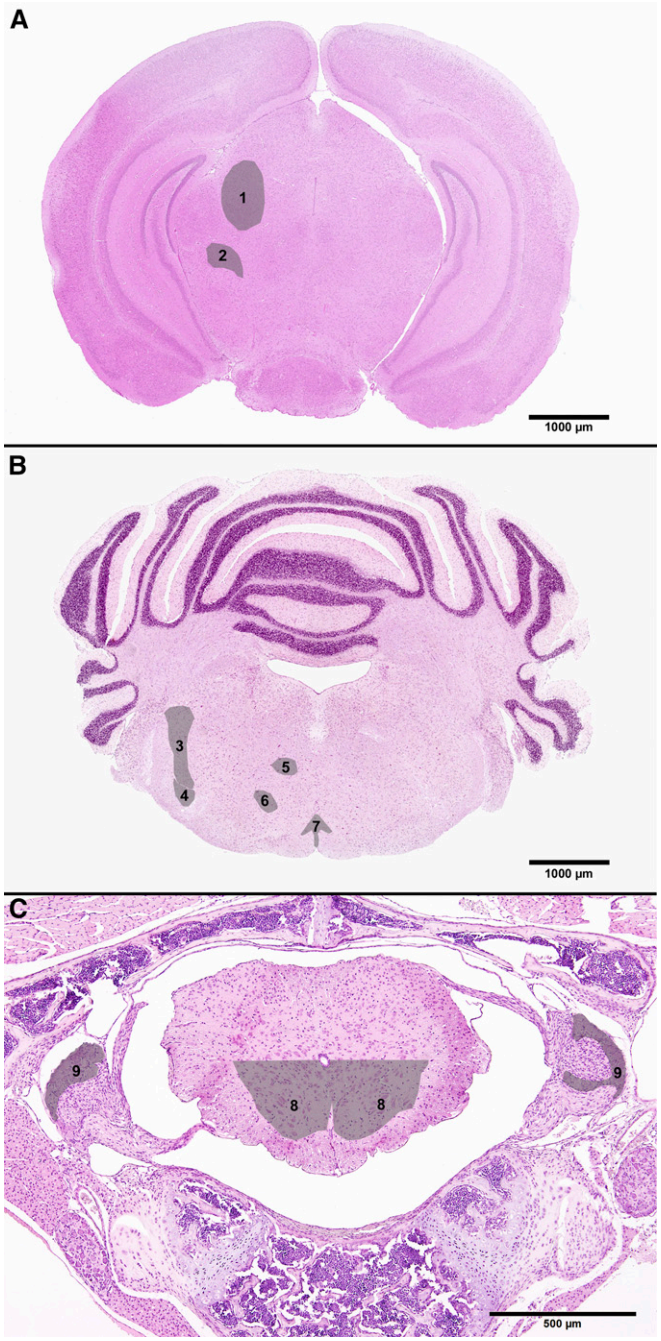

Figure 7 Affected regions in the brain stem and spinal cord of *dt-MP* (*dt/dt*) mice. (A and B) H&E stain of murine brain and (C) thoracic spinal cord. (A) One (1), anterior pretectal nucleus; 2, retroethmoid thalamic nucleus. Bar, 1000 µm. (B) Three (3), trigeminal nuclei; 4, spinal trigeminal nucleus; 5, pontine nuclei; 6, gigantocellular reticular nucleus; 7, raphe nuclei. Bar, 1000 µm. (C) Eight (8), ventral horns; 9, dorsal root ganglia. Bar, 500 µm.

skeletal muscles, and peripheral nerves of *dystonin* wild-type (+/+) mice. In *dt-MP* mice (littermates of the +/+ mice) the antigen expression was severely downregulated. Under the assumption that this antibody—which was directed against a relatively large amino acid sequence of the N terminus of a recombinant murine protein—recognizes all dystonin isoforms, the immunohistological results confirm the RT-PCR data by showing that the mutation has not only an influence on the expression of dystonin in the CNS but also in peripheral organs.

Histopathological lesions of the *dt-MP* animals consisted predominantly of axonal changes and degenerative neuronal changes, mostly restricted to sensory nuclei and to a lesser degree evident in motor nuclei. These findings emphasize most likely a primary axonopathy with subsequent damage to the neuronal cell body similar to changes observed after ischemic or traumatic axonal alterations (dying back phenomenon) (Bhanot *et al.* 2011). The degeneration of both sensory and motor neurons predominately in brain stem and spinal cord was described in former studies (Duchen *et al.* 1964; De Repentigny *et al.* 2011; Horie *et al.* 2014). Additionally, a common feature of all mutants is the unaffected cerebellum. Like in the present study, dorsal root ganglia seemed to be commonly affected. The muscle atrophy, which was described in other mouse mutants (Duchen *et al.* 1964; De Repentigny *et al.* 2011), was not evident in histological and ultrastructural investigations in the *dt-MP* mice compared to their littermates with a +/+ genotype of the same age. Nevertheless, further studies including morphometry of muscle fibers and immunohistological investigations of several intermediate filaments in skeletal muscles are needed. Thus, clinical signs of affected mice are most likely caused by axonal damage, which is regarded as the major pathological correlate of permanent functional deficits (De Stefano *et al.* 1998; Trapp *et al.* 1998; Kornek *et al.* 2000; Coleman 2005). However, chromatolysis of neurons may have caused additional secondary axonal damage.

Axonal damage was evident as formation of argyrophilic spheroids with intense immunolabeling for p-NF, n-NF, and β-APP as described earlier (Gentleman *et al.* 1993; Collard *et al.* 1995; Coleman 2005). The intense accumulation of p-NF in *dt-MP* mice indicates a disturbance of the axonal cytoskeleton, especially in the complex process of phosphorylation and dephosphorylation of neurofilaments (Meller *et al.* 1994; King *et al.* 2000). Accumulation of n-NF and immunoreactivity for β-APP is typically observed in acute and chronic white matter damage, including mechanical injury (Oehmichen *et al.* 1998), CNS virus infection like Theiler´s murine encephalomyelitis infection (Kreutzer *et al.* 2012), or mouse viral hepatitis (Dandekar *et al.* 2001) as well as multiple sclerosis (Ferguson *et al.* 1997; Kerschensteiner *et al.* 2004), human immunodeficiency virus infection (Giometto *et al.* 1997), canine distemper virus infection (Seehusen and Baumgärtner 2010), or acute intervertebral disc disease in dogs (Bock *et al.* 2013). β-APP accumulation in the proximal axonal ends occurs due to turbulences or disruption of the fast axonal transport, thus indicating functional changes of damaged axons in *dt-MP* mice. These findings support recent arguments for a role of dystonin in axonal trafficking (Bhanot *et al.* 2011). Using LFB stain, no evidence for myelin loss prior to axonal damage was observed. This was confirmed by immunohistology for myelin

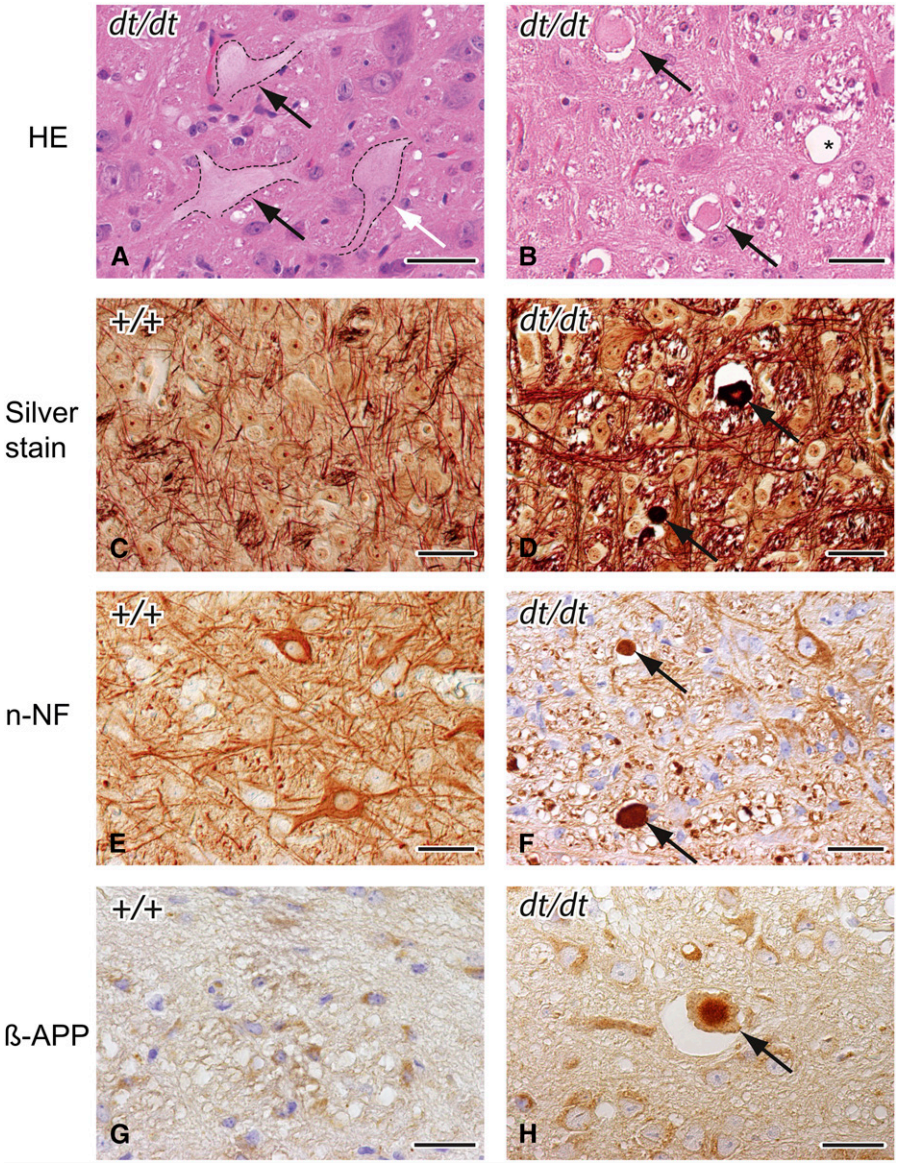

Figure 8 Histological and immunohistological findings showing neurodegeneration in *dt-MP* (*dt/dt*) animals. (A and B) H&E stain of the reticular formation of a *dt-MP* (*dt/dt*) mouse. Bar, 100 μm. (A) Degenerated neurons with chromatolysis (black arrows) and margination of the nucleus (white arrow). (B) Spheroids (arrows) representing swollen axons in dilated myelin sheaths. Asterisk: dilated myelin sheath with possible axonal dropout. (C) Normal staining of axons in the white matter of the reticular formation of a +/+ mouse; Bielschowsky's silver stain. Bar, 50 μm. (D) Severe accumulation of argyrophilic material in spheroids in the reticular formation of a *dt-MP* (*dt/dt*) mouse; Bielschowsky's silver stain (arrows). Bar, 50 μm. (E) Immunohistological staining of nonphosphorylated neurofilament (n-NF) of the cervical spinal cord in a +/+ mouse. Bar, 50 μm. (F) Marked n-NF accumulation in spheroids of the cervical spinal cord in a *dt-MP* (*dt/dt*) mouse (arrows). Bar, 50 μm. (G) Lack of axonal β-APP staining in a +/+ animal. Bar, 50 μm. (H) Immunohistological staining of β-amyloid precursor protein (β-APP) in a spheroid in a *dt-MP* (*dt/dt*) mouse (arrow). Bar, 50 μm.

basic protein. Furthermore, a role of dystonin in autophagic processes was discussed (Ferrier *et al.* 2015) because mice with a mutated *dystonin* gene showed dysfunction of autophagy within sensory neurons.

Occasional thickening and folding of myelin layers characterized ultrastructural alterations of spinal cord myelin sheaths. This finding was also seen by authors in other mouse mutants of this disease, especially in the spinal cord (Saulnier *et al.* 2002). These so-called hyper- or dysmyelinated axons were interpreted as signs of structural abnormalities of the myelin sheath in diseased mice. In contrast to dt^{Tg4} mice, the extent of myelination abnormalities in the spinal cord seemed to be less severe in *dt-MP* mice of the present study. Whether oligodendrocytes or other glial cell types like oligodendrocyte precursor cells show alterations in number and antigen expression needs to be investigated in further

Table 1 Results of special stains and immunohistology in brain stem and spinal cord of control (+/+) and *dt-MP* (*dt/dt*) mice

	Control +/+		*dt-MP* (*dt/dt*)	
Stain/antigen	Axons	Perikarya	Spheroids	Swollen perikarya
Bielschowsky's silver stain	+	—	+++	++/+++
β-Amyloid precursor protein (β-APP)	—	+	+++	+
Phosphorylated neurofilament (p-NF)	+	—	+++	++
Nonphosphorylated neurofilament (n-NF)	+/−	+++	+++	++

+, weak expression; ++, moderate expression; +++, strong expression.

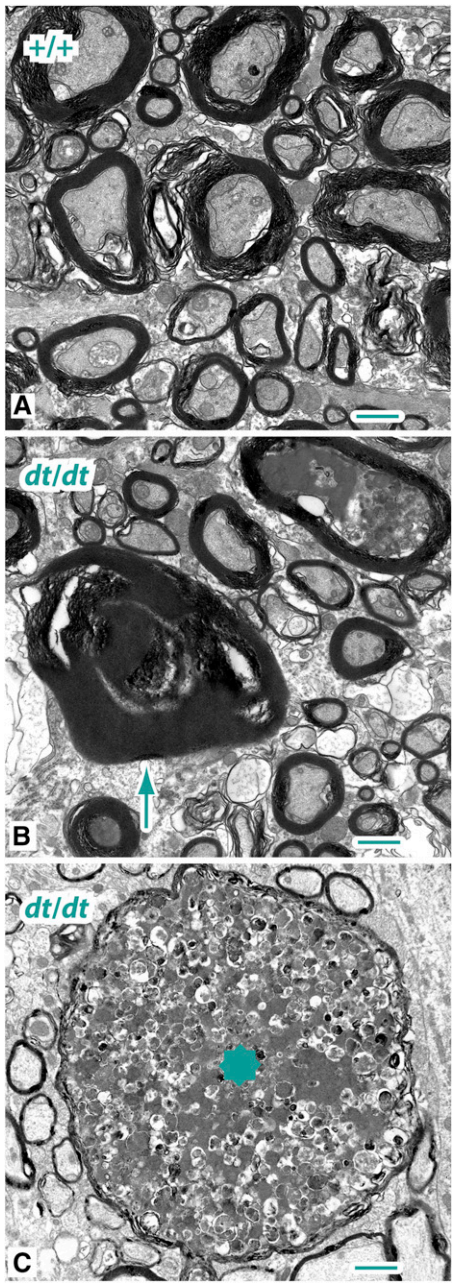

Figure 9 Electron microscopy of the central nervous system. (A) Control animal (+/+) with numerous myelinated axons. Magnification, 8000-fold. Bar, 1000 nm. (B) Hyper- and dysmyelination of axons in the spinal cord of a *dt-MP* (*dt/dt*) mouse characterized by thickening and folding of the myelin sheath. Magnification, 8000-fold. Bar, 1000 nm. (C) Spinal cord of *dt-MP* (*dt/dt*) mouse showing reduction in axon density and spheroid formation with enlarged diameter of damaged axon and accumulation of numerous cell organelles (mitochondria, dense bodies, and tubulovesicular profiles) as well as a thin myelin sheath. Magnification, 20,000-fold. Bar, 435 nm.

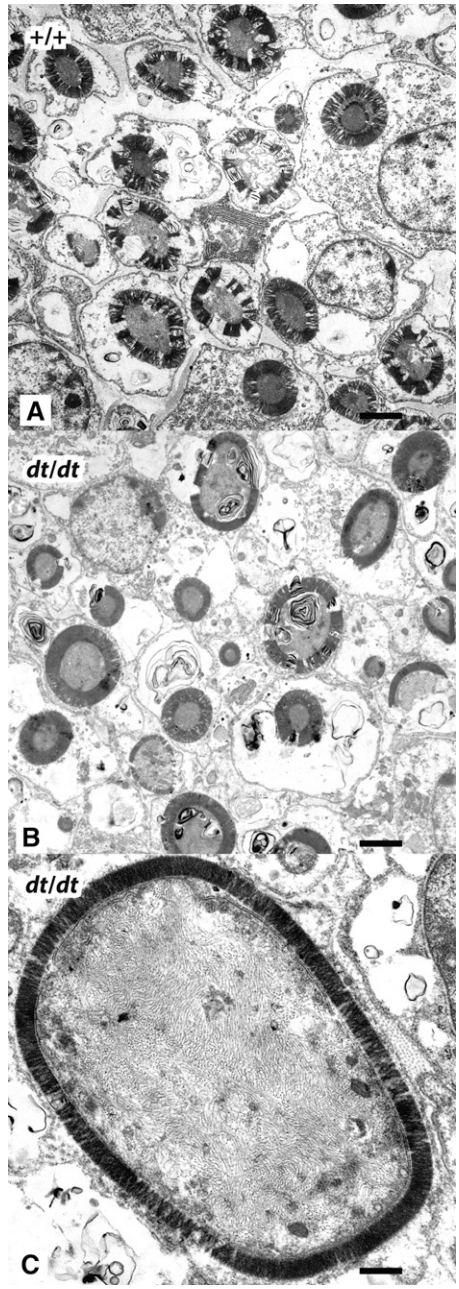

Figure 10 Electron microscopy of the peripheral nervous system. (A) *Dystonin* wild type (+/+) animal with numerous myelinated axons. Magnification, 4000-fold. Bar, 2000 nm. (B) Variation of axonal diameter and reduction in axon density in the sciatic nerve of a *dt-MP* (*dt/dt*) mouse. Magnification, 4000-fold. Bar, 2000 nm. (C) Sciatic nerve of *dt-MP* (*dt/dt*) mouse showing axon with enlarged diameter (spheroid). Magnification, 16,000-fold. Bar, 500 nm.

studies. Because demyelination is quite sparse in *dt-MP*, it can be assumed that myelin changes represent a secondary lesion that arises after the axonal damage. Additionally, mild degenerative lesions could be detected in the peripheral nerves by TEM. These results are to some extent similar to previous studies in which axonal swellings, axonal degeneration, and caliber variation of axons occurred (De Repentigny *et al.* 2003, 2011; Horie *et al.* 2014).

It remains unclear, whether the difference in the life span of dystonia musculorum mice in this study—compared to other mutations of the *dystonin* gene—is due to their genetic background, *i.e.*, modifier genes and/or environmental influences. Animals with the homozygous *dt-Alb* allele can live

for several months (Messer and Strominger 1980). Mice carrying the *BPAG1* (former name of *dystonin*) knockout allele were killed by the time they reach 5–6 weeks of age at the latest (Guo *et al.* 1995), whereas those with the *Tg4* insertion died at weaning age (Kothary *et al.* 1988), just like the *dt-MP* mutant animals of the present study.

Interestingly, *dt-MP* mice suffered from suppurative inflammation in the respiratory tract, which may have contributed to the early death of the animals. Such pneumonic changes are also described in human patients with neurodegenerative disorders like Parkinson's or Alzheimer's disease or stroke. It was supposed that aspiration pneumonia of these patients was the result of swallowing disturbances, which may be due to autonomic nervous system dysfunction (Kim *et al.* 2000; Affoo *et al.* 2013; Cereda *et al.* 2014). This feature seems to be of special interest for the present study because *dt-MP* mice showed widespread neurodegenerative lesions in the brain stem, including nuclei important for the oral and pharyngeal phase of the swallowing process, namely the trigeminal nuclei and the pontine reticular formation (Lang 2009). A predisposition for a primary or secondary bacterial infection of the respiratory tract cannot be ruled out, although there were no obvious morphological changes in the investigated lymphoid organs like lymphoid depletion or disorders of the hematopoiesis concerning the bone marrow in the *dt-MP* mice.

There are only a few reports about patients with mutations of the human *dystonin* gene (Giorda *et al.* 2004; Groves *et al.* 2010; Edvardson *et al.* 2012). The molecular origins range from single base pair deletion, point mutation, to translocation. Clinical signs like truncal ataxia, reduced muscle tonus, and in one case early death, resemble the dystonia musculorum phenotype (Messer and Strominger 1980; Kothary *et al.* 1988; Guo *et al.* 1995), but are associated with other clinical signs or a concomitant second disease. Nevertheless, the clinical phenotype as well as histological and immunohistological findings of our homozygous *dt-MP* mice and other reports (Messer and Strominger 1980; Kothary *et al.* 1988; Guo *et al.* 1995) share some features with other axonal disorders in animals and humans.

Furthermore, a recent study showed that *dystonin* mRNA was aberrantly spliced in brains of patients with Parkinson's disease (Elliott *et al.* 2012). Although molecularly not further specified, the authors demonstrated a decrease in the inclusion of *DST 1e* precursor exons and suggested a contribution of dystonin to the development of Parkinson's disease in humans.

Further research is needed to elucidate the role of the dystonin isoforms in the different tissues and to integrate dystonin in the pathomechanistic cascade of events leading to neurodegeneration in human diseases.

In summary, this study presents the identification of a new spontaneous mutation of the *dystonin* gene in C57BL/6N mice, emphasizing a disturbance of the axonal transport and of the processing of neurofilaments as important pathogenetic events.

Acknowledgments

The authors thank Johanna Barclay, Henrik Oster, Alexander Klimke, and Samir Karaca for discussions; Ronald Liem for providing the antibody; Stefanie Thiel, Monika Raabe, Uwe Plessmann, Irene Böttcher-Gajewski, Hartmut Sebesse, Jens Krull, Petra Grünig, Kerstin Rohn, and Bettina Buck for skilled technical support; the animal technicians Denise Brödner, Jennifer Flemming, and Christian Dietl for their excellent work and observations; Connie Paz for help with the manuscript; and Dirk Schaudien (Fraunhofer-Institut für Toxikologie und Experimentelle Medizin, Hannover, Germany) for scanning several slides.

Literature Cited

Affoo, R. H., N. Foley, J. Rosenbek, J. K. Shoemaker, and R. E. Martin, 2013 Swallowing dysfunction and autonomic nervous system dysfunction in Alzheimer's disease: a scoping review of the evidence. J. Am. Geriatr. Soc. 61: 2203–2213.

Bhanot, K., K. G. Young, and R. Kothary, 2011 MAP1B and clathrin are novel interacting partners of the giant cyto-linker dystonin. J. Proteome Res. 10: 5118–5127.

Bock, P., I. Spitzbarth, V. Haist, V. M. Stein, A. Tipold *et al.*, 2013 Spatio-temporal development of axonopathy in canine intervertebral disc disease as a translational large animal model for nonexperimental spinal cord injury. Brain Pathol. 23: 82–99.

Boyer, J. G., K. Bhanot, R. Kothary, and C. Boudreau-Larivière, 2010 Hearts of *Dystonia musculorum* mice display normal morphological and histological features but show signs of cardiac stress. PLoS One 5: e9465.

Cereda, E., R. Cilia, C. Klersy, M. Canesi, A. L. Zecchinelli *et al.*, 2014 Swallowing disturbances in Parkinson's disease: a multivariate analysis of contributing factors. Parkinsonism Relat. Disord. 20: 1382–1387.

Coleman, M., 2005 Axon degeneration mechanisms: commonality amid diversity. Nat. Rev. Neurosci. 6: 889–898.

Collard, J. F., F. Côté, and J. P. Julien, 1995 Defective axonal transport in a transgenic mouse model of amyotrophic lateral sclerosis. Nature 375: 61–64.

Dalpé, G., N. Leclerc, A. Vallée, A. Messer, M. Mathieu *et al.*, 1998 Dystonin is essential for maintaining neuronal cytoskeleton organization. Mol. Cell. Neurosci. 10: 243–257.

Dalpé, G., M. Mathieu, A. Comtois, E. Zhu, S. Wasiak *et al.*, 1999 Dystonin-deficient mice exhibit an intrinsic muscle weakness and an instability of skeletal muscle cytoarchitecture. Dev. Biol. 210: 367–380.

Dandekar, A. A., G. F. Wu, L. Pewe, and S. Perlman, 2001 Axonal damage is T cell mediated and occurs concomitantly with demyelination in mice infected with a neurotropic coronavirus. J. Virol. 75: 6115–6120.

De Repentigny, Y., J. Deschênes-Furry, B. J. Jasmin, and R. Kothary, 2003 Impaired fast axonal transport in neurons of the sciatic nerves from *dystonia musculorum* mice. J. Neurochem. 86: 564–571.

De Repentigny, Y., A. Ferrier, S. D. Ryan, T. Sato, and R. Kothary, 2011 Motor unit abnormalities in *Dystonia musculorum* mice. PLoS One 6: e21093.

De Stefano, N., P. M. Matthews, L. Fu, S. Narayanan, J. Stanley *et al.*, 1998 Axonal damage correlates with disability in patients with relapsing-remitting multiple sclerosis. Results of a longitudinal magnetic resonance spectroscopy study. Brain 121: 1469–1477.

Duchen, L. W., 1976 Dystonia musculorum–an inherited disease of the nervous system in the mouse. Adv. Neurol. 14: 353–365.
Duchen, L. W., S. J. Strich, and D. S. Falconer, 1964 Clinical and pathological studies of an hereditary neuropathy in mice (*Dystonia musculorum*). Brain 87: 367–378.
Edvardson, S., Y. Cinnamon, C. Jalas, A. Shaag, C. Maayan *et al.*, 2012 Hereditary sensory autonomic neuropathy caused by a mutation in dystonin. Ann. Neurol. 71: 569–572.
Elliott, D. A., W. S. Kim, S. Gorissen, G. M. Halliday, and J. B. Kwok, 2012 Leucine-rich repeat kinase 2 and alternative splicing in Parkinson's disease. Mov. Disord. 27: 1004–1011.
Ferguson, B., M. K. Matyszak, M. M. Esiri, and V. H. Perry, 1997 Axonal damage in acute multiple sclerosis lesions. Brain 120: 393–399.
Ferrier, A., Y. De Repentigny, A. Lynch-Godrei, S. Gibeault, W. Eid *et al.*, 2015 Disruption in the autophagic process underlies the sensory neuropathy in *dystonia musculorum* mice. Autophagy 11: 1025–1036.
Gentleman, S. M., M. J. Nash, C. J. Sweeting, D. I. Graham, and G. W. Roberts, 1993 Beta-amyloid precursor protein (beta APP) as a marker for axonal injury after head injury. Neurosci. Lett. 160: 139–144.
Giometto, B., S. F. An, M. Groves, T. Scaravilli, J. F. Geddes *et al.*, 1997 Accumulation of beta-amyloid precursor protein in HIV encephalitis: relationship with neuropsychological abnormalities. Ann. Neurol. 42: 34–40.
Giorda, R., A. Cerritello, M. C. Bonaglia, S. Bova, G. Lanzi *et al.*, 2004 Selective disruption of muscle and brain-specific BPAG1 isoforms in a girl with 6;15 translocation, cognitive and motor delay, and tracheo-oesophageal atresia. J. Med. Genet. 41: e71.
Goryunov, D., A. Adebola, J. J. Jefferson, C. L. Leung, A. Messer *et al.*, 2007 Molecular characterization of the genetic lesion in *Dystonia musculorum* (*dt-Alb*) mice. Brain Res. 1140: 179–187.
Groves, R. W., L. Liu, P. J. Dopping-Hepenstal, H. S. Markus, P. A. Lovell *et al.*, 2010 A homozygous nonsense mutation within the dystonin gene coding for the coiled-coil domain of the epithelial isoform of BPAG1 underlies a new subtype of autosomal recessive epidermolysis bullosa simplex. J. Invest. Dermatol. 130: 1551–1557.
Guo, L., L. Degenstein, J. Dowling, Q. C. Yu, R. Wollmann *et al.*, 1995 Gene targeting of BPAG1: abnormalities in mechanical strength and cell migration in stratified epithelia and neurologic degeneration. Cell 81: 233–243.
Hatje, K., B. Hammesfahr, and M. Kollmar, 2013 WebScipio: reconstructing alternative splice variants of eukaryotic proteins. Nucleic Acids Res. 41: W504–W509.
Horie, M., K. Watanabe, A. K. Bepari, J. Nashimoto, K. Araki *et al.*, 2014 Disruption of actin-binding domain-containing Dystonin protein causes *dystonia musculorum* in mice. Eur. J. Neurosci. 40: 3458–3471.
Kerschensteiner, M., C. Stadelmann, B. S. Buddeberg, D. Merkler, F. M. Bareyre *et al.*, 2004 Targeting experimental autoimmune encephalomyelitis lesions to a predetermined axonal tract system allows for refined behavioral testing in an animal model of multiple sclerosis. Am. J. Pathol. 164: 1455–1469.
Kim, H., C. S. Chung, K. H. Lee, and J. Robbins, 2000 Aspiration subsequent to a pure medullary infarction: lesion sites, clinical variables, and outcome. Arch. Neurol. 57: 478–483.
King, C. E., P. A. Adlard, T. C. Dickson, and J. C. Vickers, 2000 Neuronal response to physical injury and its relationship to the pathology of Alzheimer's disease. Clin. Exp. Pharmacol. Physiol. 27: 548–552.
Kornek, B., M. K. Storch, R. Weissert, E. Wallstroem, A. Stefferl *et al.*, 2000 Multiple sclerosis and chronic autoimmune encephalomyelitis: a comparative quantitative study of axonal injury in active, inactive, and remyelinated lesions. Am. J. Pathol. 157: 267–276.
Kothary, R., S. Clapoff, A. Brown, R. Campbell, A. Peterson *et al.*, 1988 A transgene containing lacZ inserted into the dystonia locus is expressed in neural tube. Nature 335: 435–437.
Kreutzer, M., F. Seehusen, R. Kreutzer, K. Pringproa, M. Kummerfeld *et al.*, 2012 Axonopathy is associated with complex axonal transport defects in a model of multiple sclerosis. Brain Pathol. 22: 454–471.
Lang, I. M., 2009 Brain stem control of the phases of swallowing. Dysphagia 24: 333–348.
Ledoux, M. S., 2011 Animal models of dystonia: lessons from a mutant rat. Neurobiol. Dis. 42: 152–161.
Leung, C. L., M. Zheng, S. M. Prater, and R. K. Liem, 2001 The BPAG1 locus: alternative splicing produces multiple isoforms with distinct cytoskeletal linker domains, including predominant isoforms in neurons and muscles. J. Cell Biol. 154: 691–697.
Meller, D., U. T. Eysel, and R. Schmidt-Kastner, 1994 Transient immunohistochemical labelling of rat retinal axons during Wallerian degeneration by a monoclonal antibody to neurofilaments. Brain Res. 648: 162–166.
Messer, A., and N. L. Strominger, 1980 An allele of the mouse mutant dystonia musculorum exhibits lesions in red nucleus and striatum. Neuroscience 5: 543–549.
Oehmichen, M., C. Meissner, V. Schmidt, I. Pedal, H. G. König *et al.*, 1998 Axonal injury: a diagnostic tool in forensic neuropathology? A review. Forensic Sci. Int. 95: 67–83.
Pool, M., C. Boudreau Larivière, G. Bernier, K. G. Young, and R. Kothary, 2005 Genetic alterations at the *Bpag1* locus in *dt* mice and their impact on transcript expression. Mamm. Genome 16: 909–917.
Röper, K., S. L. Gregory, and N. H. Brown, 2002 The 'Spectraplakins': cytoskeletal giants with characteristics of both spectrin and plakin families. J. Cell Sci. 115: 4215–4225.
Sanger, F., S. Nicklen, and A. R. Coulson, 1977 DNA sequencing with chain-terminating inhibitors. Proc. Natl. Acad. Sci. USA 74: 5463–5467.
Saulnier, R., Y. De Repentigny, V. W. Yong, and R. Kothary, 2002 Alterations in myelination in the central nervous system of dystonia musculorum mice. J. Neurosci. Res. 69: 233–242.
Seehusen, F., and W. Baumgärtner, 2010 Axonal pathology and loss precede demyelination and accompany chronic lesions in a spontaneously occurring animal model of multiple sclerosis. Brain Pathol. 20: 551–559.
Trapp, B. D., J. Peterson, R. M. Ransohoff, R. Rudick, S. Mörk *et al.*, 1998 Axonal transection in the lesions of multiple sclerosis. N. Engl. J. Med. 338: 278–285.
Young, K. G., and R. Kothary, 2008 Dystonin/Bpag1 is a necessary endoplasmic reticulum/nuclear envelope protein in sensory neurons. Exp. Cell Res. 314: 2750–2761.

Communicating editor: T. R. Magnuson

GENETICS

Supporting Information
www.genetics.org/lookup/suppl/doi:10.1534/genetics.116.186932/-/DC1

Axonopathy in the Central Nervous System Is the Hallmark of Mice with a Novel Intragenic Null Mutation of *Dystonin*

Frauke Seehusen, Kirsten Kiel, Stefano Jottini, Peter Wohlsein, Andre Habierski, Katharina Seibel, Tanja Vogel, Henning Urlaub, Martin Kollmar, Wolfgang Baumgärtner, and Ulrike Teichmann

DOI: 10.1534/genetics.116.186932

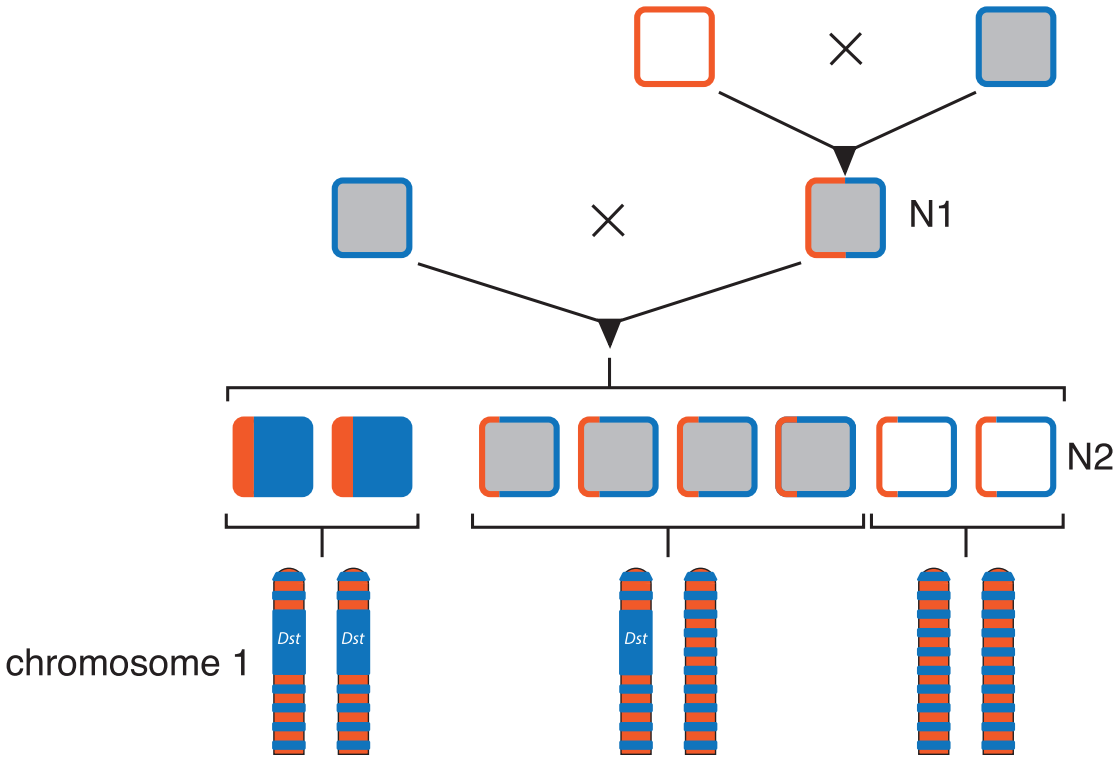

Figure S1. Linkage analysis

A positive-proven C57BL/6N carrier animal (symbol outlined in blue with gray inside) was mated to an FVB/N mouse (symbol outlined in orange). The resulting N1 positive-proven carrier animal (outlined half blue, half orange with gray inside) was mated to a positive-proven C57BL/6N carrier animal. N2 offspring animals had 75% C57BL/6N and 25% FVB/N genome. Phenotypically apparent mice (blue and orange filled symbols) were homozygous and carried a 28 Mb long region resulting from C57BL/6N genome only. The region was analysed in silico and contained the mutated *dystonin* gene (blue area in the depicted chromosome). Carrier animals (outlined half blue, half orange with gray inside) were heterozygous.

Figure S2: Nucleotide and amino acid sequences in wild type *dystonin* and *dt-MP* alleles

(A) The sequence shows the genomic region of the *dystonin* gene (GenBank accession number NC_000067.5) from the end of exon 39 (included only in the short *dystonin* transcript variants *dystonin-e* and *dystonin-n*) to the beginning of exon 40 (included only in the long

dystonin transcript variants). (B) In the *dt-MP* mouse mutant, the genomic region from close to the end of exon 39 up to intron 61 is deleted. Translation of putative short *dystonin* transcripts would lead to different C-termini, compared to the known *dystonin-e* and *dystonin-n* variants, disrupting the penultimate plectin-repeat and removing the last plectin-repeat of the IFBD1 domain.

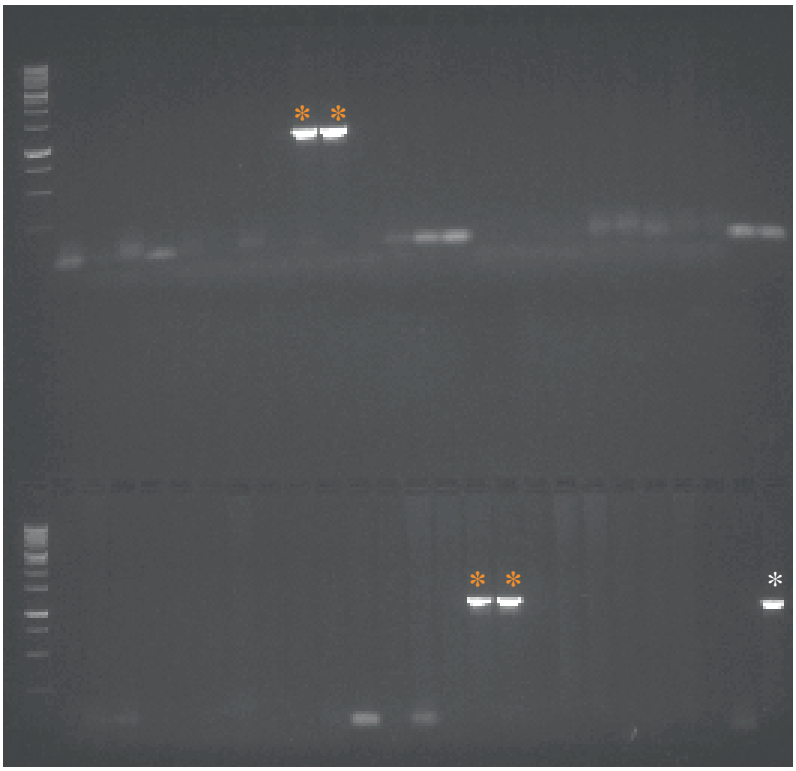

Figure S3. Genotyping the originally purchased animals

Only two out of 25 breeding pairs are carrier animals of the mutant *dt-MP* allele (red asterisks). White asterisk: positive control.

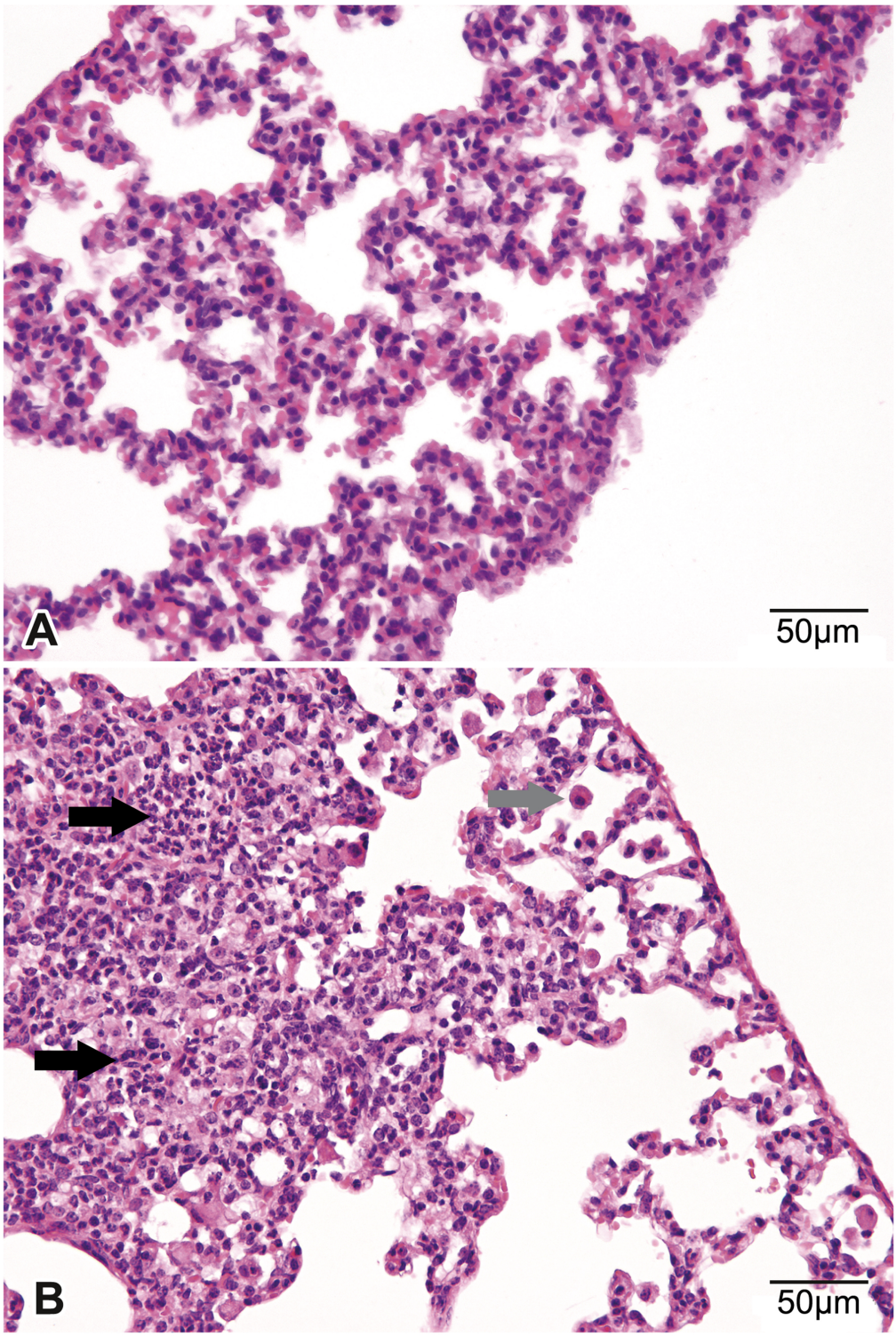

Figure S4. Lesions in peripheral organs of *dt-MP* mice. Hematoxylin eosin (HE) stain of the lung tissue in a *dystonin* wild type (+/+) control (A) and a *dt-MP* (*dt/dt*) mouse (B). (B) Moderate multifocal intraalveolar accumulation of neutrophils (black arrows) and prominent alveolar macrophages (grey arrow) in lung of a *dt-MP* animal. Bars = 50 µm.

Supplemental information

All PCR protocols had 30 cycles starting with an initial denaturation at 94°C for 30 seconds. Annealing and elongation conditions are given at each primer pair. Each PCR started with an initial denaturation at 94°C for 3 minutes and ended with a final elongation at 72°C for 6 minutes.

Name	Sequence	5'-position *	Annealing	Elongation	Reference
Fig. 3a					
Exon43-f	5'-GCC AGA GGC TTC TGC TCT ATG-3'	281064	62°C, 45 s	72°C, 50 s	Pool et al., 2005 (IFBD2)
Exon43-r	5'-CAG GGC GGG GGA ATA GTC AAA GAC AGA-3'	281648			
Deletion-f	5'-GCT GGT GGA CGA GGG CTT CG-3'	274333	62°C, 45 s	72°C, 90 s	
Deletion-r	5'-TGC CAT GCT GTG CAC AGC AGC-3'	315018			
Control-f	5'-AGA CCG CCG GTG ACG TAT CAG G-3'	272159	62°C, 45 s	72°C, 50 s	
Control-r	5'-GGT CGT GAC TTC TGT ATG CAT GCC-3'	272885			
Fig. 3b					
Wild type allele-f	5'-GCA GGC AGT GAT GTC CTC TGC-3'	275227	62°C, 45 s	72°C, 45 s	
Wild type allele-r	5'-CTA CCC CGT TAG CAT TAC AGC C-3'	275887			
dt-MP-allele-f	5'-GCT GGT GGA CGA GGG CTT CG-3'	274333	62°C, 45 s	72°C, 90 s	
dt-MP-allele-r	5'-TGC CAT GCT GTG CAC AGC AGC-3'	315018			
Fig. 5					
dystonin-f**	5'-ATT CAA GAG TTC ATG GAC CTA CGG ACA C-3'	265943			
dystonin-a-r	5'-TAA TTA GGC GGT TTT CAG TCT GGG TGA G-3'	288987	68°C, 45 s	72°C, 45 s	Leung et al., 2001
dystonin-b-r	5'-CAA TAA GGC CTC TTA AAA CTG CCT GAA A-3'	279758	68°C, 45 s	72°C, 45 s	Leung et al., 2001
dystonin-e/n-r	5'-TC ACG ATC GTC TCC AGC TCA CGG-3'	269797	68°C, 45 s	72°C, 45 s	Leung et al., 2001

*with respect to coding strand, genomic DNA
** common forward primer for all isoforms

S1 data. Primers
Fig. 3A: Primer sequences to identify the deletion in genomic DNA. Primers binding in exon 43 (coding for the IFDB2) show a band in control, but not in affected animals. Primers binding in exon 39 and intron 61, respectively, give a band in affected animals. The internal control band spans from exon 38 via intron 38 to exon 39.
Fig. 3C: Primer sequences for genotyping. The dystonin wild type allele is detected with primers binding in introns 39 and 40. The dt-MP allele is detected with primers that bind upstream of the deletion start in exon 39 and downstream of the end in intron 61, respectively.
Fig. 4: Primer sequences to detect the different dystonin transcripts in cDNA. For all isoforms, a common intron-spanning forward primer binding in exon 36/37 was used. The backward primers bind in exon 48 (dystonin-a), exon 43 (dystonin-b) and exon 38 (dystonin-e/n), respectively.